The *Escherichia coli* PriA Helicase Has Two Nucleotide-Binding Sites Differing Dramatically in Their Affinities for Nucleotide Cofactors. 1. Intrinsic Affinities, Cooperativities, and Base Specificity of Nucleotide Cofactor Binding†

Aaron L. Lucius, Maria J. Jezewska, and Wlodzimierz Bujalowski*

Department of Biochemistry and Molecular Biology, Department of Obstetrics and Gynecology, The Sealy Center for Structural Biology, Sealy Center for Cancer Cell Biology, The University of Texas Medical Branch at Galveston, 301 University Boulevard, Galveston, Texas 77555-1053

Received September 9, 2005; Revised Manuscript Received March 8, 2006

ABSTRACT: Interactions of the *Escherichia coli* PriA helicase with nucleotide cofactors have been studied using the fluorescence titration and analytical ultracentrifugation techniques. Binding of unmodified cofactors was characterized by the fluorescence competition titration method. The obtained data establish that at saturation the PriA helicase binds two nucleotide molecules per protein monomer. This result corroborates with the primary structure of the protein, which contains sequence motifs implicated as putative nucleotide-binding sites. The intrinsic affinities of the binding sites differ by 2−4 orders of magnitude. Thus, the PriA helicase has a strong and a weak nucleotide-binding site. The binding sites differ dramatically in their properties. The strong site is highly specific for adenosine cofactors, while the weak site shows very modest base specificity. The affinities of the strong and weak binding sites for ATP are lower than the affinities for ADP, although both sites have similar affinity for the inorganic phosphate group. Unlike the weak site, the affinity of the strong site profoundly depends on the structure of the phosphate group of the ATP cofactor. Binding of unmodified nucleotides indicates the presence of positive cooperative interactions between bound cofactors (i.e., the existence of communication between the two sites). Magnesium cations are specifically involved in controlling the cofactor affinity for the strong site, while the affinity of the weak site is predominantly determined by interactions between the phosphate group and ribose regions of the cofactor and the protein matrix. The significance of these results for the activities of the PriA helicase is discussed.

The *Escherichia coli* primosome is a multi-protein complex that catalyzes the priming of the DNA during the replication process (*1*−*14*). Two helicases in the *E. coli* cell, DnaB and PriA proteins, are involved in the functioning of the primosome, and both enzymes participate in propelling the translocation of the primosome along DNA during synthesis of short oligoribonucleotide primers, which are used to initiate synthesis of the complementary strand. The PriA protein also plays a fundamental role in the ordered assembly of the primosome (*1, 4, 11, 12*). Moreover, the enzyme is involved in recombination and repair processes in the *E. coli* cell (*1*−*18*).

The PriA protein displays multiple activities that reflect complex interactions of the enzyme with different ingredients of the primosome and the replication fork, including protein−protein and protein−DNA interactions (*1, 2, 4, 15*−*20*). These activities include ATPase and dATPase activities strongly stimulated by a specific DNA fragment termed the primosome assembly site (PAS)[1] (*1, 2, 4, 7, 9, 19, 20*), nonspecific binding to the ssDNA and specific strong binding to the PAS-DNA sequence (*7*−*10, 21, 22*), and 3′ → 5′ helicase activity that can be specifically stimulated by PAS (*11, 12*). The native protein is a monomer with a molecular weight of 81.7 kDa, and the monomer is the predominant form of the protein in solution (*7*−*9, 21, 22*).

In vivo functions of the PriA protein as a helicase are related to the ability of the enzyme to interact with both ss and dsDNA in the duplex DNA unwinding reaction, which is fueled by the hydrolysis of nucleoside triphosphates (NTPs) (*3, 7, 11*−*21*). A helicase performs a complex free-energy transduction process, where the binding and/or hydrolysis of NTPs regulate enzyme activity and affinity toward different conformations of the DNA (*3, 23*−*25*). Surprisingly, although the importance of interactions of the PriA helicase with nucleotide cofactors has been recognized, the nature of these interactions remains completely obscure. Such fundamental aspects of PriA−cofactor interactions such as the number of nucleotide-binding sites; intrinsic affinities

† This work was supported by NIH Grant GM-46679 (to W.B.). A.L.L. was partially supported by a J. B. Kempner postdoctoral fellowship.

* Corresponding author. Tel.: (409)772-5634. Fax: (409)772-1790. E-mail.: wbujalow@utmb.edu.

[1] Abbreviations: TNP-ATP, 2′(3′)-*O*-(2,4,6-trinitrophenyl)adenosine triphosphate; TNP-ADP, 2′(3′)-*O*-(2,4,6-trinitrophenyl)adenosine 5′-diphosphate; NTP, nucleoside triphosphate; AMP-PNP, β,γ-imidoadenosine 5′-triphosphate; AMP-PCP, β,γ-methylenadenosine 5′-triphosphate; ATP, adenosine 5′-triphosphate; ADP adenosine 5′-diphosphate; GDP, guanosine 5′-diphosphate; CDP, cytosine 5′-diphosphate; TDP, thymidine 5′-diphosphate; PAS, primosome assembly site; Tris, tris-(hydroxymethyl)aminomethane; DTT, dithiothreitol; EDTA, ethylenediaminetetraacetic acid disodium salt.

10.1021/bi051826m CCC: $33.50
Published on Web 05/20/2006

of ATP, ADP, and inorganic phosphate; possible cooperative interactions among the binding sites; base specificity of the site(s); and effect of solution conditions, including salt and magnesium, on intrinsic and cooperative interactions have never been addressed. Elucidation of nucleotide interactions with the PriA helicase is of paramount importance for our understanding of the activities of the enzyme including the translocation of the helicase on the DNA lattice, duplex DNA unwinding, formation and translocation of the primosome, and the involvement of the enzyme in the restarting of stalled replication forks (*1*−*4*, *17*−*20*).

In this paper, we report extensive and quantitative analyses of the interactions of the PriA helicase with nucleotide cofactors. This is the first determination of the energetics and stoichiometry of the nucleotide binding to the enzyme. We present direct evidence that the PriA helicase has two nucleotide-binding sites that can engage in interactions with the cofactors and have dramatically different properties. The intrinsic affinities of the sites differ by 2−4 orders of magnitude. The strong binding site is highly specific for adenosine cofactors, while the weak site shows only modest base specificity. Nevertheless, the presence of positive cooperative interactions between bound cofactors indicates complex communication between the sites. Mg^{2+} cations are specifically involved in controlling the cofactor affinity for the strong nucleotide-binding site of the enzyme.

MATERIALS AND METHODS

Reagents and Buffers. All solutions were made with distilled and deionized >18 MΩ (Milli-Q Plus) water. All chemicals were reagent grade. Buffer C is 10 mM sodium cacodylate adjusted to pH 7.0 with HCl, 1 mM DTT, and 25% glycerol. Selection of 25% glycerol in the buffer results from the fact that the PriA protein stability is significantly increased at higher glycerol concentration (*21*, *22*). Temperatures and concentrations of salts in the buffer are indicated in the text.

PriA Protein. The *E. coli* PriA protein has been isolated and purified as we described before (*21*, *22*). The enzyme was >98% pure as judged by polyacrylamide electrophoresis with Coomassie Brilliant Blue staining. The concentration of the protein was spectrophotometrically determined, with an extinction coefficient $\epsilon_{280} = 1.06 \times 10^5$ cm^{-1} M^{-1} (monomer), determined using an approach based on the Edeldoch method (*21*, *22*, *26*−*29*).

Nucleotides. TNP-ATP and TNP-ADP were from Molecular Probes (Eugene, OR) (*30*). ATP was from CalBiochem; ADP, GDP, CDP, and TDP were from Sigma (St. Louis, MO). All nucleotides used in the binding studies were >95% pure as judged by TLC on silica (*28*, *30*).

Fluorescence Measurements. All steady-state fluorescence titrations were performed using the Fluorolog F-11 spectrofluorometer (Jobin Yvon). To avoid possible artifacts, due to the fluorescence anisotropy of the sample, polarizers were placed in excitation and emission channels and set at 90° and 55° (magic angle), respectively (*21*, *22*, *31*−*33*). The cofactor binding was followed by monitoring the PriA protein fluorescence ($\lambda_{ex} = 300$ nm, $\lambda_{em} = 340$ nm). Computer fits were performed using Mathematica (Wolfram, IL) and KaleidaGraph (Synergy Software, PA). All titration points were corrected for dilution and inner filter effects using the following formula (*28*, *34*, *35*):

$$F_{i_{cor}} = (F_i - B_i)\left(\frac{V_i}{V_o}\right)10^{0.5b(A_{i\lambda ex}+A_{i\lambda em})} \quad (1)$$

where $F_{i_{cor}}$ is the corrected value of the fluorescence intensity at a given point of titration; F_i is the experimentally measured fluorescence intensity; B_i is the background; V_i is the volume of the sample at a given titration point; V_o is the initial volume of the sample; b is the total length of the optical path of the sample expressed in cm; and $A_{i\lambda_{ex}}$ and $A_{i\lambda_{em}}$ are the absorbances of the sample at excitation and emission wavelengths, respectively (*34*, *35*). The relative fluorescence quenching, ΔF_{obs}, of the PriA protein emission upon binding of a nucleotide cofactor is defined as $\Delta F_{obs} = (F_o - F_{i_{cor}})/F_o$, where F_i is the fluorescence of the protein at a given titration point, and F_o is the initial value of the fluorescence of the sample (*21*, *22*, *31*−*33*).

Quantitative Examination of the PriA Helicase−TNP-ADP and −TNP-ATP Binding Isotherms. In this work, we followed the binding of TNP-modified nucleotide cofactors to the PriA helicase by monitoring the quenching, ΔF_{obs}, of the protein emission. Quantitative method for quantitatively estimating the total average degree of binding ($\Sigma\Theta_i$; number of nucleotide molecules bound per PriA monomer) and the free nucleotide concentration (N_F) has been previously described in detail by us (*31*−*33*, *35*, *36*). Briefly, the experimentally observed ΔF_{obs} has a contribution from each of the different possible "*i*" complexes of the PriA protein with the cofactor. Thus, the observed fluorescence quenching is functionally related to $\Sigma\Theta_i$ by

$$\Delta F_{obs} = \Sigma\Theta_i \Delta F_{i_{max}} \quad (2)$$

where $\Delta F_{i_{max}}$ is the molecular parameter characterizing the molar fluorescence quenching of the PriA helicase with the nucleotide cofactor bound in complex *i*. The same value of ΔF_{obs} obtained at two different total helicase concentrations, P_{T1} and P_{T2}, indicates the same physical state of the protein, i.e., the degree of binding, $\Sigma\Theta_i$, and the free nucleotide concentration (N_F) must be the same. The values of $\Sigma\Theta_i$ and N_F are then related to the total nucleotide concentrations (N_{T1} and N_{T2}) and the total protein concentrations (P_{T1} and P_{T2}) at the same value of ΔF_{obs} by

$$\Sigma\Theta_i = \frac{N_{T2} - N_{T1}}{P_{T2} - P_{T1}} \quad (3a)$$

$$N_F = N_{Tx} - (\Sigma\Theta_i)P_{Tx} \quad (3b)$$

where $x = 1$ or 2 (*31*−*33*, *35*, *36*).

Analytical Ultracentrifugation Measurements. Sedimentation velocity experiments were performed with an Optima XL-A analytical ultracentrifuge (Beckman Inc., Palo Alto, CA) using double-sector charcoal-filled 12 mm centerpieces as described before (*37*−*39*). Sedimentation velocity scans of the TNP-ADP−PriA sample were collected at the absorption band of the TNP moiety (445 nm).

RESULTS

Maximum Stoichiometry of the PriA Helicase−Nucleotide Cofactor Complex. Formation of the complex between the

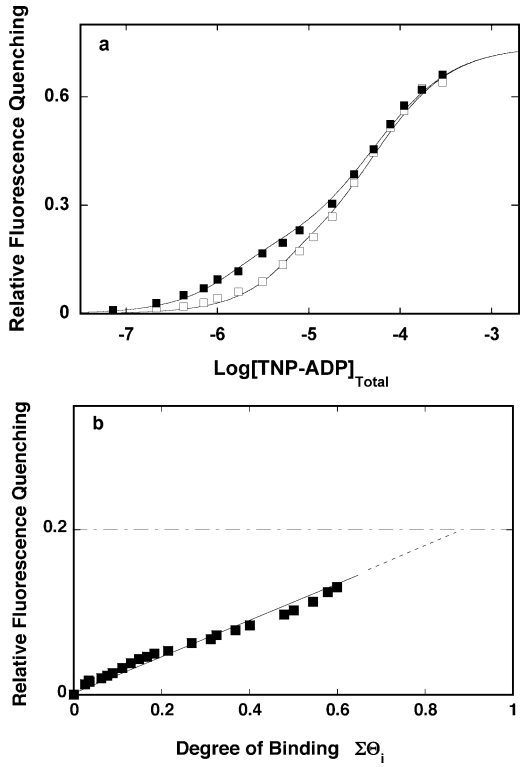

FIGURE 1: (a) Fluorescence titrations of the PriA protein with TNP-ADP in buffer C (pH 7.0, 20 °C) containing 20 mM NaCl and 5 mM $MgCl_2$ at different enzyme concentrations: (■) 1.0×10^{-6} M; (□) 6.2×10^{-6} M. The solid lines are nonlinear least-squares fits of the titration curves, according to the model of two different, discrete, and cooperative binding sites (eqs 4−6) using a single set of binding parameters: $K_1 = 1.5 \times 10^6$ M^{-1}, $K_2 = 1.9 \times 10^4$ M^{-1}, $\sigma = 1$, $\Delta F_1 = 0.2$, and $\Delta F_2 = 0.55$. (b) Dependence of the relative fluorescence quenching, ΔF_{obs}, upon the average degree of binding of TNP-ADP on the PriA helicase, $\Sigma\Theta_i$, in the high-affinity binding phase (■). The values of $\Sigma\Theta_i$ have been determined using the quantitative method described in Materials and Methods. The solid line follows the experimental points and does not have a theoretical basis. The dashed line is an extrapolation of $\Sigma\Theta_i$ to the value of ΔF_{obs} corresponding to the intermediate plateau of the high-affinity binding phase (− - −).

unmodified nucleotide cofactors and the PriA helicase is not accompanied by a change of the protein fluorescence that is adequate to perform quantitative analysis of the binding process (data not shown). However, we found that binding of nucleotide analogues, TNP-ATP and TNP-ADP, where the TNP moiety has an absorbance band that overlaps with the tryptophan emission spectrum of the PriA protein, is accompanied by a strong quenching of the protein fluorescence, which provides the required signal to monitor the complex association process (*28*, *35*, *40*). Fluorescence titrations of the PriA protein with TNP-ADP, at two different protein concentrations, in buffer C (pH 7.0, 20 °C), containing 20 mM NaCl and 5 mM $MgCl_2$ are shown in Figure 1a. The maximum quenching of the protein fluorescence at saturation is 0.75 ± 0.1. The large error in the determined maximum quenching value results from the fact that we could not reach the complete plateau at saturation, due to the precipitation of the helicase−cofactor complex, which occurs at very high TNP-ADP concentrations (Figure 1a) (see below).

A striking feature of the spectroscopic titration curves in Figure 1a is the clear presence of two binding phases; the high- and low-affinity binding phase. This is particularly noticeable for the titration performed at low protein concentration, where the total concentration of TNP-ADP, $[TNP\text{-}ADP]_{Total}$, approaches the concentration of the free cofactor, $[TNP\text{-}ADP]_{Free}$ (*28*, *35*, *36*, *41*). The same two binding phases are even more pronounced in the case of the PriA−ssDNA complex (*64*). The plot indicates that the intermediate plateau of the titration curve is characterized by a relative quenching of the protein fluorescence of ∼0.20 ± 0.03; thus, saturation of the high-affinity phase induces an ∼20% quenching of the protein fluorescence. On the other hand, the low affinity phase is characterized by an additional protein fluorescence quenching of ∼0.55 ± 0.08. Notice, the heterogeneity of the binding process is also clearly evident from the fact that the titration curve at low protein concentration extends over more than 2 orders of magnitude of [TNP-ADP] (Figure 1a) (*28*, *35*, *36*).

The selected protein concentration provides separation of the binding isotherms up to a quenching value of ∼0.14. To quantitatively obtain the total average degree of binding, $\Sigma\Theta_i$, within the high-affinity phase, the fluorescence titration curves, shown in Figure 1a have been analyzed using the method outlined in Materials and Methods (*28*, *35*, *36*). The dependence of the observed relative fluorescence quenching, ΔF_{obs}, upon the total average degree of binding, $\Sigma\Theta_i$, of TNP-ADP on the PriA helicase is shown in Figure 1b. The plot is, within the experimental accuracy, linear. The separation of the titration curves allows us to obtain the values of $\Sigma\Theta_i$ up to ∼0.6 TNP-ADP molecules per PriA monomer. Short extrapolation to the value of the quenching in the high-affinity binding phase, $\Delta F_1 = 0.20 \pm 0.03$, provides the stoichiometry of the complex as 0.9 ± 0.1. Therefore, the obtained data show that, in the high-affinity phase, the PriA monomer binds one molecule of TNP-ADP.

Examination of the low-affinity phase in the same way as the high-affinity phase would require significantly higher protein concentrations to obtain adequate separation of the spectroscopic titration curves (*28*, *35*, *36*). However, as pointed out above, such studies are hindered by the precipitation of the protein−cofactor complex at high [PriA] and high [TNP-ADP]. Therefore, the stoichiometry of the PriA−TNP-ADP complex in the low-affinity phase, and by the same token the maximum stoichiometry of the helicase−nucleotide cofactor complex, has been examined using an independent sedimentation velocity approach, as described previously (*37*−*39*). The TNP-ADP analogue has absorption bands between ∼400 and 500 nm, allowing us to monitor the sedimentation of the cofactor and its complex with the helicase without any interference from the protein absorption. The experiments were performed at an elevated salt concentration to avoid any precipitation of the sample (see below).

Sedimentation velocity scans of TNP-ADP (monitored at 445 nm) in the presence of the PriA helicase are shown in Figure 2. The total concentration of the PriA protein and TNP-ADP are 5.3×10^{-6} M and 7.3×10^{-5} M, respectively. Fluorescence titration curves and the salt effect on the nucleotide binding to the helicase, discussed below, indicate that in these solution conditions and at the selected total concentrations of the nucleotide and the helicase, $[TNP\text{-}ADP]_T$ and $[PriA]_T$, we should observe ∼80% saturation of the PriA protein with the cofactor. The fast moving boundary in Figure 2 corresponds to the TNP-ADP−PriA complex

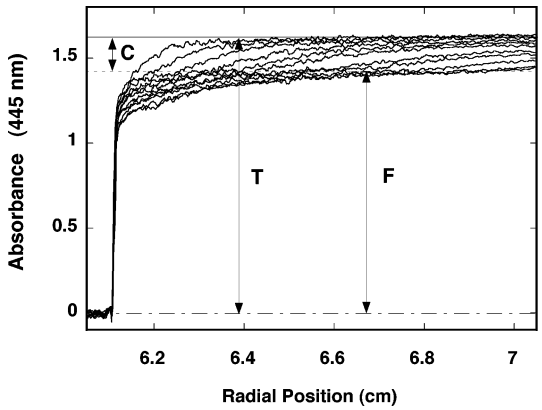

FIGURE 2: Sedimentation velocity absorption profiles at 445 nm of TNP-ADP in the presence of the PriA helicase in buffer C (pH 7.0, 20 °C) containing 20 mM NaCl and 5 mM $MgCl_2$. Concentrations of TNP-ADP and the PriA protein are 7.3×10^{-5} M and 5.3×10^{-6} M, respectively. The scans were collected at 30 000 rpm. The short initial parts of the scans correspond to the buffer−air region above the meniscus. The arrows indicate the absorption of the total concentration of TNP-ADP (T), the concentration of the cofactor bound in the complex with the PriA protein (C), and the concentration of the free TNP-ADP (F). The horizontal lines indicate the locations of the plateaus corresponding to the zero line, (− - −), free TNP-ADP concentration (- - -), and total TNP-ADP concentration (−).

(*37*). The slow moving boundary corresponds to the sedimentation of the free TNP-ADP. At the applied rotational speed of 30 000 rpm, the sedimentation boundary of the free TNP-ADP only slightly moves from the meniscus. From the total absorption of the initial scans (*T*), that corresponds to the total concentration of TNP-ADP, and the absorption of the slow moving boundary (*F*), one can directly calculate the absorption of the TNP-ADP bound to the helicase, as $C = T - F$. Thus, the concentration of the cofactor bound to the PriA protein is $(C/T) \times [\text{TNP-ADP}]_T$ (i.e., a fraction of the total cofactor concentration). The determined total average degree of binding is then $\Sigma\Theta_i = [(C/T) \times [\text{TNP-ADP}]_T)/[\text{PriA}]_T] = 1.7 \pm 0.2$, which constitutes (85 ± 12) % of the maximum saturation, in excellent agreement with the fluorescence titration data. Thus, the obtained results indicate that one additional molecule of nucleotide cofactor binds to the PriA helicase in the low-affinity binding phase. In other words, these data establish that, at saturation, the PriA helicase binds two nucleotide molecules.

Heterogeneity in Macroscopic Affinities of the Nucleotide-Binding Sites of the PriA Helicase. As mentioned above, a characteristic feature of the fluorescence titration curve at low PriA concentration, where the $[\text{TNP-ADP}]_{\text{Total}}$ is close to the $[\text{TNP-ADP}]_{\text{Free}}$, is that the titration curves extend over more than 2 orders of magnitude of the nucleotide concentration (i.e., between ∼10% and ∼90% of the total observed fluorescence change) (*28*, *35*, *36*). If the two nucleotide-binding sites of the PriA helicase had the same affinity for the cofactor, then the free cofactor concentration cannot span more than 2 orders of magnitude between 10% and ∼90% of the entire binding process (*35*, *36*, *41*). In other words, a binding system of two discrete binding sites, without heterogeneity in their intrinsic affinities, cannot generate such behavior. Therefore, these results unambiguously show that the macroscopic affinities of the nucleotide cofactors for the PriA helicase are a decreasing function of the total degree of binding, $\Sigma\Theta_i$ (see the Discussion).

Statistical Thermodynamic Model for the Nucleotide Cofactor Binding to the PriA Helicase. The thermodynamic data described above show that the PriA helicase binds two nucleotide molecules and that the binding is characterized by a strongly decreasing macroscopic affinity with the increase of the total average degree of binding. Because of the heterogeneous structure of a protein molecule, even at the primary structure level, the two nucleotide-binding sites must be not only energetically but also structurally different (see the Discussion). Therefore, the simplest statistical thermodynamic model (i.e., the model containing the fewest number of parameters) that can account for the observed binding process is that the PriA helicase has two distinct nucleotide-binding sites, characterized by different intrinsic affinities and described by intrinsic binding constants (K_{B_1} and K_{B_2}). However, analyses of the unmodified cofactor binding indicate that the sites are not completely independent (i.e., they also exhibit cooperative interactions between them that depend on the type of the nucleotide) (see below). The cooperative interactions can phenomenologically be accounted for by the cooperative interaction parameter, σ.

The partition function, *Z*, describing the binding of two nucleotide cofactors to the PriA helicase is then defined as

$$Z = 1 + (K_{B_1} + K_{B_2})L_F + K_{B_1}K_{B_2}\sigma L_F^2 \qquad (4)$$

where L_F is the free nucleotide cofactor concentration. The total average degree of binding, $\Sigma\Theta_i$, is defined as

$$\Sigma\Theta_i = \frac{(K_{B_1} + K_{B_2})L_F + 2K_{B_1}K_{B_2}\sigma L_F^2}{Z} \qquad (5)$$

The experimentally observed fluorescence quenching, ΔF_{obs}, expressed in terms of the partial quenching parameters, ΔF_1 and ΔF_2, characterizing each individual binding site, and the binding parameters K_{B_1}, K_{B_2}, and σ is then

$$\Delta F_{\text{obs}} = \frac{(\Delta F_1 K_{B_1} + \Delta F_2 K_{B_2})L_F + (\Delta F_1 + \Delta F_2)K_{B_1}K_{B_2}\sigma L_F^2}{Z} \qquad (6)$$

There are five parameters (ΔF_1, ΔF_2, K_{B_1}, K_{B_2}, and σ) in eq 6. However, some of these parameters can directly be determined from the titration curves and the plot in Figure 1b, utilizing the fact that the two binding sites differ very strongly in their affinities (Figure 1a). The value of $\Delta F_1 = 0.20 \pm 0.03$ is obtained directly from the high-affinity phase in Figure 1a and the plot of ΔF_{obs} as a function of the average degree of binding, as $\Delta F_1 = \partial\Delta F_{\text{obs}}/\partial\Sigma\Theta_i$ (Figure 1b). The value of $\Delta F_2 = \Delta F_{\text{max}} - \Delta F_1$, where ΔF_{max} is the maximum of the observed fluorescence quenching ($\Delta F_{\text{max}} = 0.74 \pm 0.1$). The titration curves in Figure 1a provide $\Delta F_2 = 0.55 \pm 0.08$. The value of the intrinsic binding constant, K_{B_1}, can be obtained from the initial slope of the plot of the average degree of binding as a function of the free TNP-ADP concentration that provides $K_{B_1} = (1.5 \pm 0.5) \times 10^6$ M^{-1} (data not shown). Thus, there are only two remaining parameters, K_{B_2} and σ, that must be determined. The obtained values of all parameters are included in Table 1. The intrinsic binding constant for the second site $K_{B_2} = (1.9 \pm 0.6) \times 10^4$ M^{-1}; thus, it is 2 orders of magnitude lower than the

Table 1: Maximum Number of Nucleotide-Binding Sites (n), Intrinsic Binding Constants (K_{B_1} and K_{B_2}), Cooperativity Parameter (σ), and Fluorescence Quenching Parameters (ΔF_1 and ΔF_2) for Binding of Nucleotide Anaglogues (TNP-ADP and TNP-ATP) to Two Nucleotide Sites of the *E. coli* PriA Helicase in Buffer C (pH 7.0, 20 °C) Containing 20 mM NaCl in the Presence of 5 mM $MgCl_2$ or 0.1 mM EDTA

cofactor	n	K_{B_1} (M^{-1})	K_{B_2} (M^{-1})	σ	ΔF_1	ΔF_2
TNP-ADP + 5 mM $MgCl_2$	2	$(1.5 \pm 0.5) \times 10^6$	$(1.9 \pm 0.6) \times 10^4$	1 ± 0.3	0.2 ± 0.03	0.54 ± 0.08
TNP-ADP + 0.1 mM EDTA	2	$(5.1 \pm 1.2) \times 10^7$	$(3.7 \pm 1.1) \times 10^5$	1 ± 0.3	0.2 ± 0.03	0.64 ± 0.05
TNP-ATP + 5 mM $MgCl_2$	2	$(4.3 \pm 1.5) \times 10^6$ [a]				
TNP-ATP + 0.1 mM EDTA	2	$(1.0 \pm 0.3) \times 10^8$	$(7.8 \pm 1.6) \times 10^5$	1 ± 0.3	0.18 ± 0.03	0.59 ± 0.05

[a] Determined in kinetic measurement (see ref *63*).

value of K_{B_1}. Also, in the case of TNP-ADP, the parameter $\sigma = 1.0 \pm 0.3$, indicating that the binding of the cofactor analogue to two nucleotide-binding sites of the PriA helicase is virtually independent (see below). We could not extend the same analysis to TNP-ATP in the presence of Mg^{2+} because the enzyme slowly hydrolyzes the ATP analogue on the time scale comparable with the time necessary to collect the equilibrium titration curve (data not shown).

Binding of the Unmodified ATP and ADP to the PriA Helicase. To quantitatively determine the interaction parameters of the unmodified ATP and ADP with the PriA helicase, we applied the competition titration method, described previously by us (*28*, *32*, *33*, *42*). In this approach, the PriA protein is titrated with the reference nucleotide analogue (e.g., TNP-ADP) in the absence and in the presence of the unmodified nucleotide (e.g., ADP or ATP). The observed signal originates only from the binding of the "reference" cofactor to the enzyme. However, in the presence of unmodified nucleotide, the titration curve is affected by the interaction of the unmodified nucleotide with the enzyme, providing a means to characterize these interactions (*28*, *42*).

Fluorescence titrations of the PriA protein with TNP-ADP in the absence and in the presence of 1 mM ADP in buffer C (pH 7.0, 20 °C), containing 20 mM NaCl and 5 mM $MgCl_2$, are shown in Figure 3a. The concentration of the helicase is 1×10^{-6} M. There are two important qualitative aspects of the presented titration curves. First, the presence of ADP shifts the titration curve toward a higher TNP-ADP concentration range in the high-affinity phase, a clear indication that both nucleotides compete for the same binding site on the enzyme. Second, in the low-affinity phase, the curve is not shifted toward a higher TNP-ADP concentration, as would be expected for a simple competitive binding, but toward lower [TNP-ADP]. Such an asymmetric shift of the isotherm in the presence of a competing ligand indicates positive cooperative interactions between the reference ligand, TNP-ADP, and the unmodified cofactor, ADP, and/or between ADP molecules, bound to the PriA helicase (*28*,*42*). Thus, in terms of cooperative interactions, the unmodified ADP behaves differently than its TNP-modified analogue (see the Discussion). Moreover, the maximum quenching of the protein fluorescence, at saturation, is higher in the presence of ADP than in the absence of the competing cofactor (Figure 3a).

In the absence of ssDNA, the PriA helicase does not hydrolyze unmodified ATP on the time scale of the equilibrium binding experiment, to any significant extent, in the applied solution conditions. This property of the enzyme allowed us to perform the analogous competition binding analysis using unmodified ATP. Fluorescence titrations of the PriA helicase with TNP-ADP in the absence and in the presence of 0.5 mM ATP are shown in Figure 3b. The

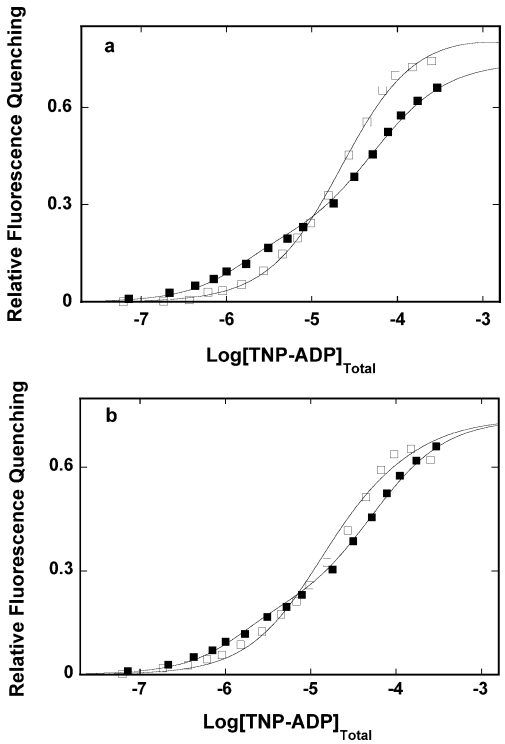

FIGURE 3: (a) Fluorescence titrations of the PriA helicase with TNP-ADP in buffer C (pH 7.0, 20 °C) containing 20 mM NaCl and 5 mM $MgCl_2$ in the absence (■) and in the presence of 1 mM ADP (□). The concentration of PriA helicase is 1×10^{-6} M. The solid lines are nonlinear least-squares fits of the titration curves, according to the model of two discrete cooperative binding sites for two competing ligands (eqs 7−10), using binding parameters for ADP included in Table 2, and with $\Delta F_3 = 0.2$ and $\Delta F_4 = 0.84$. The spectroscopic and binding parameters for the reference nucleotide, TNP-ADP, are the same as in Figure 1a. (b) Fluorescence titration of the PriA helicase with TNP-ADP in buffer C (pH 7.0, 20 °C), containing 20 mM NaCl and 5 mM $MgCl_2$, in the absence (■) and in the presence of 0.5 mM ATP (□). The concentration of PriA helicase is 1×10^{-6} M. The solid lines are nonlinear least-squares fits of the titration curves, according to the model of two discrete cooperative binding sites for two competing ligands (eqs 7−10), using binding parameters for ADP included in Table 2, and with $\Delta F_3 = 0.2$ and $\Delta F_4 = 0.87$. The spectroscopic and binding parameters for the reference nucleotide, TNP-ADP, are the same as in Figure 1a.

behavior of the system in the presence of ATP is similar to that observed for ADP, indicating the presence of cooperative interactions (see above) (*28*, *42*). However, in the presence of ATP, the titration curve is less shifted to a higher concentration of the reference ligand, TNP-ADP, in the high-affinity phase than observed in the presence of ADP. Thus, the data show that, independent of any binding model, ATP has a lower macroscopic affinity for the strong nucleotide-binding site than ADP.

Analysis of Competitive Cooperative Ligand Binding to Two Discrete Cooperative Binding Sites. In the presence of the reference ligand, TNP-ADP, and competing unmodified ligand (e.g., ADP or ATP), each nucleotide-binding site of the PriA helicase can exist in three different states: free, bound with TNP-ADP, or bound with unmodified nucleotide. Such complex binding systems can be most efficiently described using the matrix method to obtain the expressions for the partition function, Z_C, and the total average degree of binding, $\Sigma\Theta_i$, for the reference nucleotide in terms of its intrinsic binding parameters and the intrinsic binding parameters of the unmodified, competing cofactor (*41*,*44*). The partition function of the total binding system, Z_C, is defined as

$$Z_C = (1\ 0\ 0)\ \mathbf{M}_1\ \mathbf{M}_2 \begin{pmatrix} 1 \\ 1 \\ 1 \end{pmatrix} \tag{7}$$

where $\mathbf{M}_1$ and $\mathbf{M}_2$ are the transfer matrices that correlate the statistical weights of different states for the first and the second nucleotide-binding site of the enzyme. These are three-state matrices, defined individually for each discrete binding site, as (*41*, *44*)

$$\mathbf{M}_1 = \begin{pmatrix} 1 & K_{B_1}L_R & K_{1C}L_C \\ 1 & \sigma K_{B_1}L_R & \sigma_{RC}K_{1C}L_C \\ 1 & \sigma_{RC}K_{B_1}L_R & \sigma_C K_{1C}L_C \end{pmatrix} \tag{8a}$$

and

$$\mathbf{M}_2 = \begin{pmatrix} 1 & K_{B_2}L_R & K_{2C}L_C \\ 1 & \sigma K_{B_2}L_R & \sigma_{RC}K_{2C}L_C \\ 1 & \sigma_{RC}K_{B_2}L_R & \sigma_C K_{2C}L_C \end{pmatrix} \tag{8b}$$

where K_{B_1}, K_{B_2}, and σ are the intrinsic binding constants and cooperative interaction parameter that characterize the binding of reference nucleotide (TNP-ADP), as discussed above (eq 4); L_R is the free concentration of the reference nucleotide (TNP-ADP); K_{1C}, K_{2C}, and σ_C are the intrinsic binding constants and cooperative interaction parameter that characterize the binding of the competing cofactor; L_C is the free concentration of the competing cofactor; σ_C is the parameter characterizing cooperative interactions between the bound molecules of the competing cofactor; and σ_{RC} is the parameter that characterizes cooperative interactions between the reference and the competing nucleotide, respectively (*41*, *44*). The total average degree of binding, $\Sigma\Theta_i$, is then

$$\Sigma\Theta_i = \frac{\left[(1\ 0\ 0)\left[\dfrac{\partial(\mathbf{M}_1\mathbf{M}_2)}{\partial \ln L_R}\right]\begin{pmatrix} 1 \\ 1 \\ 1 \end{pmatrix}\right]}{Z_C} \tag{9}$$

The observed relative fluorescence quenching, ΔF_{obs}, is generated only from the complexes containing the reference ligand (TNP-ADP) and is defined as

$$\Delta F_{obs} = \frac{(1\ 0\ 0)\left\{\left[\dfrac{\partial(\mathbf{M}_1\mathbf{M}_2)}{\partial \ln (K_{B_1}L_R)}\right]\begin{pmatrix} \Delta F_1 \\ \Delta F_1 \\ \Delta F_3 \end{pmatrix} + \left[\dfrac{\partial(\mathbf{M}_1\mathbf{M}_2)}{\partial \ln (K_{B_1}L_R)}\right]\begin{pmatrix} \Delta F_2 \\ \Delta F_2 \\ \Delta F_4 \end{pmatrix}\right\}}{Z_C} \tag{10}$$

where ΔF_3 and ΔF_4 are the relative fluorescence quenching values characterizing the complexes of the PriA helicase with two different cofactors bound at different sites. Notice, this is an extremely complex system, and there are 11 parameters—ΔF_1, ΔF_2, ΔF_3, ΔF_4, K_{B_1}, K_{B_2}, σ, K_{1C}, K_{2C}, σ_C, and σ_{RC}—in eqs 7−10 that characterize the observed binding process. However, ΔF_1, ΔF_2, K_{B_1}, K_{B_2}, and σ are independently determined from fluorescence titration of the PriA protein with TNP-ADP in the absence of the competing cofactor. Therefore, there are six remaining parameters—ΔF_3, ΔF_4, K_{1C}, K_{2C}, σ_C, and σ_{RC}—that have to be determined. This is still a formidable number of parameters, and some reasonable approximations are necessary.

The titration curves in panels a and b of Figure 3 indicate that the value of ΔF_3 is not strongly affected, if at all, by the presence of ADP or ATP (i.e., binding of the unmodified cofactor to the weak site does not affect the fluorescence quenching induced by the TNP-ADP bound at the strong site). Therefore, the value of ΔF_3 can be approximated as equal to ΔF_1. The value of ΔF_4 cannot be lower than the highest value of the observed fluorescence quenching (e.g., in Figure 3a, $\Delta F_{obs} \approx 0.76$, but cannot be larger than 1, which is the maximum physically possible value of the relative fluorescence quenching). This imposes a very limited range ($\pm$ 15%) on the values of ΔF_4, which is taken as the average between the maximum observed quenching for a particular cofactor and 1. The final simplifying assumption is that the values of the cooperativity parameters, σ_C, and σ_{RC}, are the same between unmodified cofactor molecules and between the reference and the unmodified cofactor. This is justified by the fact that the shift of the isotherm toward lower TNP-ADP concentrations (Figure 3), in the low-affinity phase of the titration curves, is only moderate indicating that the values of both σ_C and σ_{RC} are not much higher than 1 (see below). The solid lines in panels a and b of Figure 3 are nonlinear least-squares fits of the spectroscopic binding curves using eqs 7−10 and K_{1C}, K_{2C}, and $\sigma_{RC} = \sigma_C$ as fitting parameters. The obtained binding parameters for ADP and ATP are included in Table 2.

The data indicate that the intrinsic affinity of ATP for the strong nucleotide-binding site of the PriA helicase is characterized by $K_{1C} = (7 \pm 4) \times 10^4\ M^{-1}$, which is by a factor of ~30 lower than $K_{1C} = (2.0 \pm 0.8) \times 10^6\ M^{-1}$ obtained for ADP in the examined solution conditions. The intrinsic affinity for the weak binding site is ~2 and ~4 orders of magnitude lower for both ATP and ADP as compared to the strong binding site. On the other hand, the weak site shows much less preference for ADP as compared to ATP, with the value of K_{2C} being only a factor of ~2 higher for ADP than the value obtained for ATP (Table 2). Unlike the TNP-ADP analogue, where the binding process is essentially noncooperative (Figure 1a, Table 1), binding of both ATP and ADP is characterized by a moderate positive cooperativity with $\sigma_C \approx 3.3-3.8$ (see the Discussion).

Base Specificity of the Two Nucleotide-Binding Sites of the PriA Helicase. Analogous ligand competition studies

Table 2: Maximum Number of Binding Sites (n), Intrinsic Binding Constants (K_{1C} and K_{2C}), and Cooperativity Parameter (σ_C) for the Binding of Different Nucleotide Cofactors and Inorganic Phosphate Group (PO^{4-}) to two Nucleotide-Binding Sites of the *E. coli* PriA Helicase in Buffer C (pH 7.0, 20 °C), Containing 20 mM NaCl and 5 mM $MgCl_2$[a]

cofactor	n	K_{1C} (M^{-1})	K_{2C} (M^{-1})	σ_C
ATP	2	$(7.0 \pm 2.5) \times 10^4$	$(0.8 \pm 0.4) \times 10^2$	3.3 ± 1.2
ADP	2	$(2.0 \pm 0.8) \times 10^6$	$(1.5 \pm 0.6) \times 10^2$	3.8 ± 1.4
dATP	2	$(9.0 \pm 2.9) \times 10^5$	$(3.5 \pm 1.4) \times 10^2$	3.8 ± 1.4
dADP	2	$(1.0 \pm 0.4) \times 10^6$	$(5.0 \pm 1.8) \times 10^2$	$3.5 \pm 1.$
PO^{4-}		$(1.0 \pm 0.4) \times 10^2$	$(1.0 \pm 0.4) \times 10^2$	0.5 ± 0.3
GDP	2	$(6.5 \pm 2.5) \times 10^3$	$(0.4 \pm 0.2) \times 10^2$	5.0 ± 2.6
CDP	2	$(2.0 \pm 0.8) \times 10^3$	$(0.3 \pm 0.12) \times 10^2$	2.3 ± 1.1
TDP	2	$(3.0 \pm 1.1) \times 10^3$	$(0.2 \pm 0.1) \times 10^2$	4.0 ± 1.9
UDP	2	$(7.0 \pm 2.5) \times 10^3$	$(0.2 \pm 0.1) \times 10^2$	4.1 ± 1.9
ATPγS	2	$(9.0 \pm 3.5) \times 10^3$	$(2.8 \pm 1.1) \times 10^2$	1.0 ± 0.4
AMP-PNP	2	$(4.0 \pm 1.3) \times 10^3$	$(0.3 \pm 0.12) \times 10^2$	3.0 ± 1.5
AMP-PCP	2	$(3.0 \pm 1.1) \times 10^3$	$(0.2 \pm 0.1) \times 10^2$	4.0 ± 1.9

[a] See the text for details.

have been performed with various nucleotide cofactors, differing by the type of base, to evaluate the base specificity of the strong and weak nucleotide-binding site of the PriA helicase (*28*, *29*, *42*−*44*). Fluorescence titrations of the PriA protein with TNP-ADP in the presence of 1 mM GDP are shown in Figure 4a. For comparison, the titration of the enzyme with TNP-ADP, in the absence of GDP, is also included. The titration curve is little affected in the high-affinity phase by the presence of 1 mM GDP, indicating that the cofactor has a much lower affinity for the strong binding site than does ADP (Figure 3a). However, the shift of the titration curve in the low-affinity phase is more pronounced than the same shift in the case of ADP, indicating a higher value for the cooperativity parameter, σ_C, than observed for ADP. Fluorescence titrations of the PriA protein with TNP-ADP in the presence of 1 mM CDP, in the same solution conditions, is shown in Figure 4b. The data indicate that CDP has the affinity for the strong binding site similar to GDP; however, only a slight shift of the low-affinity phase toward lower [TNP-ADP] indicates that the value of σ_C must be lower than observed for GDP. Analyses of the titration curves in panels a and b of Figure 4 have been performed in the same way as described above for the competition studies of unmodified ADP and ATP. The solid lines in panels a and b of Figure 4 are nonlinear least-squares fits of the fluorescence titration curves using eqs 7−10 and K_{1C}, K_{2C}, and $\sigma_{RC} = \sigma_C$ as fitting parameters. Analogous titrations and analyses have been performed for a series of nucleotide cofactors and inorganic phosphate, and the corresponding binding parameters for all examined cofactors are included in Table 2. It is evident that ADP has an intrinsic affinity for the strong nucleotide-binding site of the PriA helicase that is ∼2−3 orders of magnitude higher when compared to all other cofactors with a different base. However, there is little preference for the adenosine base at the weak nucleotide-binding site where the affinities are within a factor of ∼10 among different cofactors (see the Discussion). Also, although the cooperativity parameter σ_C is the highest for GDP, its value differs only by a factor of ∼2 among different unmodified cofactors. The intrinsic affinities of the inorganic phosphate group, PO^{4-}, is the same for both binding sites with $K_{1C} = K_{2C} \approx 100$ M^{-1} and is the lowest among all studied ligands (see the Discussion).

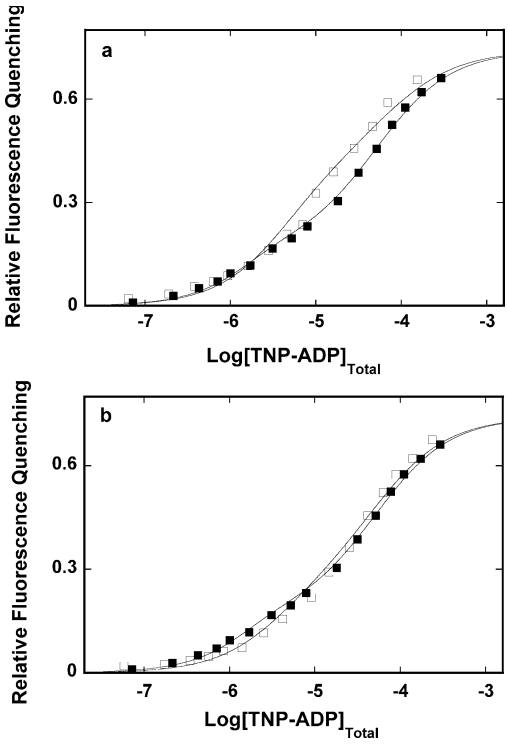

FIGURE 4: (a) Fluorescence titration of the PriA helicase with TNP-ADP in buffer C (pH 7.0, 20 °C), containing 20 mM NaCl and 5 mM $MgCl_2$, in the absence (■) and in the presence of 1 mM GDP (□). The concentration of PriA helicase is 1×10^{-6} M. The solid lines are nonlinear least-squares fits of the titration curves, according to the model of two discrete cooperative binding sites for two competing ligands (eqs 7−10), using binding parameters for GDP included in Table 2, and with $\Delta F_3 = 0.2$ and $\Delta F_4 = 0.95$. The spectroscopic and binding parameters for the reference nucleotide, TNP-ADP, are the same as in Figure 1a. (b) Fluorescence titration of the PriA helicase with TNP-ADP in buffer C (pH 7.0, 20 °C), containing 20 mM NaCl and 5 mM $MgCl_2$, in the absence (■) and in the presence of 2 mM CDP (□). The concentration of PriA helicase is 1×10^{-6} M. The solid lines are nonlinear least-squares fits of the titration curves, according to the model of two discrete cooperative binding sites for two competing ligands (eqs 7−10), using binding parameters for CDP included in Table 2, and with $\Delta F_3 = 0.2$ and $\Delta F_4 = 0.90$. The spectroscopic and binding parameters for the reference nucleotide, TNP-ADP, are the same as in Figure 1a.

Role of the ATP Phosphate Groups and Ribose in Interactions of Nucleotide Cofactors with the Two Nucleotide-Binding Sites of the PriA Helicase. The fact that in the case of some helicases only nucleotide triphosphates can induce a high-affinity state of the protein for the ssDNA indicates that the γ-phosphate is involved in complex allosteric interactions that extend beyond the nucleotide-binding site(s) (*23*−*25*, *28*). To address the question of the effect of the specific structure of the ATP phosphate group on the cofactor binding to the PriA helicase, we performed competition titration studies using various ATP analogues, differing in the structure of the phosphate group.

Fluorescence titrations of the PriA helicase with TNP-ADP in the presence of two different ATPγS concentrations in buffer C (pH 7.0, 20 °C) containing 20 mM NaCl and 5 mM $MgCl_2$ are shown in Figure 5. Inspection of the plots clearly shows a different behavior as compared to ATP or unmodified nucleoside diphosphates (Figures 3b, 4a, and 4b). As the ATP analogue concentration increases, the entire titration curve shifts toward higher TNP-ADP concentrations,

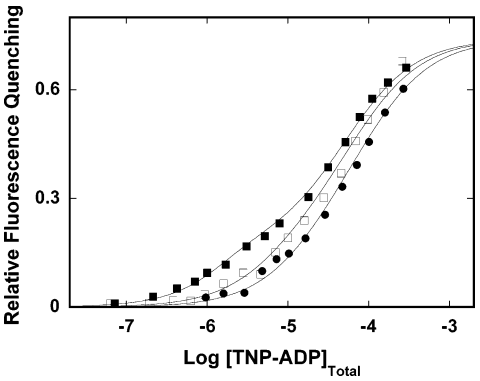

FIGURE 5: (a) Fluorescence titration of the PriA helicase with TNP-ADP in buffer C (pH 7.0, 20 °C), containing 20 mM NaCl and 5 mM $MgCl_2$, in the absence and in the presence of different ATPγS concentrations: (■) 0 mM, (□) 1 mM, (●) 3 mM. The concentration of PriA helicase is 1×10^{-6} M. The solid lines are nonlinear least-squares fits of the titration curves, according to the model of two discrete cooperative binding sites for two competing ligands (eqs 7−10), using binding parameters for ATPγS included in Table 2. The spectroscopic and binding parameters for the reference nucleotide, TNP-ADP, are the same as in Figure 1a.

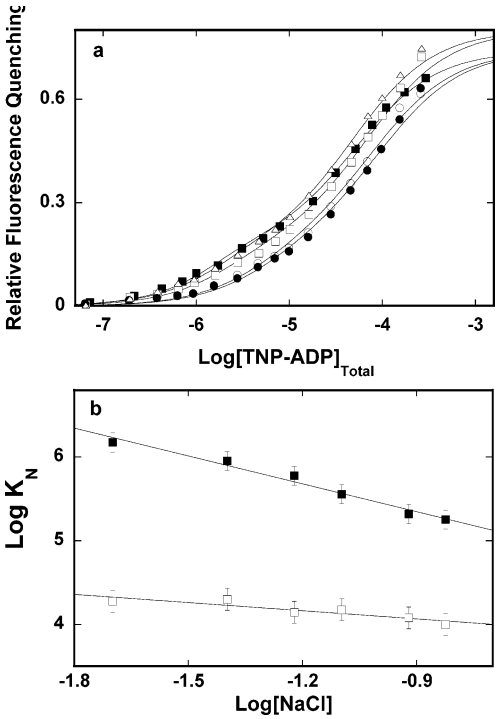

FIGURE 6: (a) Fluorescence titrations of the PriA helicase with TNP-ADP in buffer C (pH 7.0, 20 °C), containing 5 mM $MgCl_2$ and different concentrations of NaCl: (■) 20 mM, (△) 40 mM, (□) 60 mM, (○) 120 mM, and (●) 150 mM. The concentration of the PriA helicase is 1×10^{-6} M. The solid lines are nonlinear least-squares fits of the titration curves, according to the model of two different, discrete, and cooperative binding sites, defined by eqs 4−6. (b) The dependence of the logarithm of the intrinsic binding constant, K_1 (■) and K_2 (□), for the TNP-ADP binding to the PriA helicase upon the logarithm of [NaCl]. The solid lines indicate the slopes of the plots, $\partial \log K_1/\partial \log [NaCl] = -1.1$ and $\partial \log K_2/\partial \log [NaCl] = -0.3$, respectively (see the text for details).

indicating that ATPγS efficiently competes with TNP-ADP at selected ATP analogue concentrations for both nucleotide-binding sites of the helicase. The solid lines in Figure 5 are nonlinear least-squares fits of the experimental titration curves according to the model of two competing, cooperatively binding ligands (eqs 7−10) using a single set of binding and spectroscopic parameters with the same quenching parameters, ΔF_1 and ΔF_2, as obtained for the titrations with TNP-ADP in the absence of cofactor. Similar studies have been performed with AMP-PNP and AMP-PCP, and the obtained binding parameters are included in Table 2.

Although ATPγS has the highest affinity for the strong nucleotide-binding site among all examined ATP analogues, the values of the intrinsic binding constant, K_{1C}, for all examined ATP analogues are significantly lower than the value of K_{1C} obtained for ATP (Table 2). The situation is different for the weak binding site where ATPγS has an affinity higher by a factor of ∼3.5 than ATP, while AMP-PNP and AMP-PCP have significantly lower affinities than ATP. On the other hand, there are clear differences in the value of the cooperative interaction parameter, σ_C, among the ATP analogues. While the binding of the ATPγS is noncooperative with $\sigma_C = 1.0 \pm 0.3$, the binding of the AMP-PNP and AMP-PCP is characterized by σ_C values of 3.0 ± 1.5 and 4.0 ± 1.9, much closer to the value of the same parameter obtained for ATP (see the Discussion).

Competition studies with dATP and dADP have been performed in an analogous way, and the obtained binding parameters are included in Table 2. Both cofactors bind to the two nucleotide-binding sites of the PriA helicase with moderate positive cooperativity (Table 2). Binding of dATP to the strong site is characterized by the intrinsic binding constant $K_{1C} \approx 9 \times 10^5$ M^{-1} (i.e., significantly larger than the value of $K_{1C} \sim 7 \times 10^4$ M^{-1} observed for ATP). On the other hand, dADP binds to the strong site with the affinity similar to ADP. Nevertheless, both adenosine deoxyribonucleotides have affinity for the strong site higher by ∼2−3 orders of magnitude than the affinities of the cofactors with different bases. The affinities of dATP and dADP for the weak binding site are higher than the corresponding affinities of ATP and ADP, nonetheless, lower by 3−4 orders of magnitude than the affinities of the same cofactors for the strong binding site.

Salt Effect on the Nucleotide Cofactor Binding to the Strong and Weak Nucleotide-Binding Sites of the PriA Helicase. To gain insight into the nature of the two nucleotide-binding sites, we examined the salt effect on the energetics of the nucleotide cofactor binding to both binding sites of the PriA helicase. These studies have been performed using the TNP-ADP analogue. Fluorescence titrations of PriA protein with TNP-ADP in buffer C (pH 7.0, 20 °C) containing 5 mM $MgCl_2$ and different NaCl concentrations are shown in Figure 6a. The effect is complex and includes both changes in the fluorescence quenching parameters, ΔF_1 and ΔF_2, and the binding parameters, K_{B_1}, K_{B_2}, and σ. Analyses of the titration curves, in the same way as described above (Figure 1a), indicate that the apparent shift of the titration curves at lower salt concentration, up to 60 mM NaCl, results exclusively from the increased values of ΔF_1 and ΔF_2 (data not shown). Further increase of the salt concentration shifts the titration curves toward the higher TNP-ADP concentration range, clearly indicating a decreasing macroscopic affinity of the cofactor.

Figure 6b shows the dependence of the logarithm of the intrinsic binding constants, K_{B_1} and K_{B_2}, of the TNP-ADP binding to the PriA helicase upon the logarithm of the NaCl concentration (log−log plot) (*45*, *46*). Within the experi-

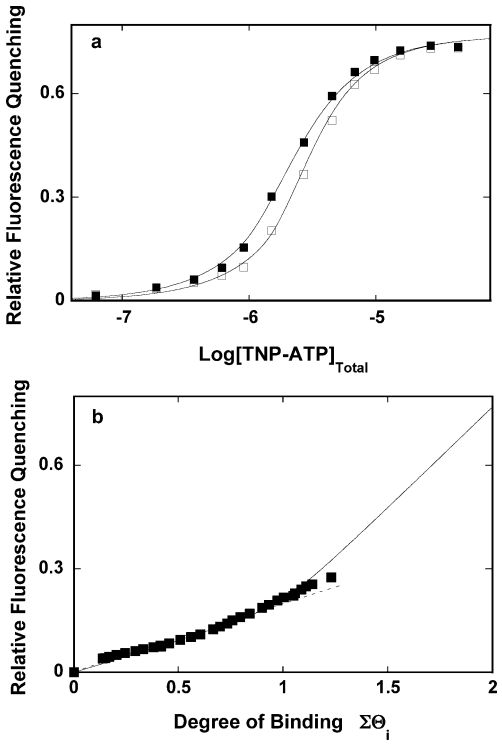

FIGURE 7: (a) Fluorescence titration of the PriA protein with TNP-ATP in buffer C (pH 7.0, 20 °C), containing 20 mM NaCl and 0.1 mM EDTA at different enzyme concentrations: (■) 1.0×10^{-6} M, (□) 1.5×10^{-6} M. The solid lines are nonlinear least-squares fits of the titration curves, according to the model of two different, discrete and cooperative binding sites (eqs 4−6) using a single set of binding parameters: $K_1 = 1.0 \times 10^8$ M^{-1}, $K_2 = 7.8 \times 10^5$ M^{-1}, $\sigma = 1$, $\Delta F_1 = 0.18$, and $\Delta F_2 = 0.59$. (b) Dependence of the relative fluorescence quenching, ΔF_{obs}, upon the average degree of binding of TNP-ADP on the PriA helicase, $\Sigma\Theta_i$ (■). The values of $\Sigma\Theta_i$ have been determined using the quantitative method described in Materials and Methods. The solid line is the theoretical dependence of ΔF_{obs}, upon $\Sigma\Theta_i$, generated using the spectroscopic and binding parameters included in panel a. The dashed line is extrapolation of ΔF_{obs} to the value of $\Sigma\Theta_i = 1$ (see the text for details).

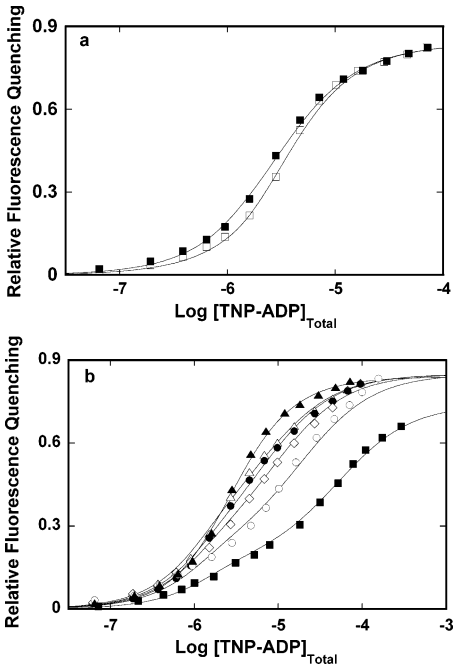

FIGURE 8: (a) Fluorescence titration of the PriA protein with TNP-ADP in buffer C (pH 7.0, 20 °C), containing 20 mM NaCl and 0.1 mM EDTA at different enzyme concentrations: (■) 1.0×10^{-6} M, (□) 1.5×10^{-6} M. The solid lines are nonlinear least-squares fits of the titration curves, according to the model of two different, discrete and cooperative binding sites (eqs 4−6) using a single set of binding parameters: $K_1 = 5.1 \times 10^7$ M^{-1}, $K_2 = 3.7 \times 10^5$ M^{-1}, $\sigma = 1$, $\Delta F_1 = 0.20$, and $\Delta F_2 = 0.64$. (b) Fluorescence titration of the PriA helicase with TNP-ADP in buffer C (pH 7.0, 20 °C), containing 20 mM NaCl and different concentrations of $MgCl_2$: (▲) 0 mM, (△) 0.05 mM, (●) 0.1 mM, (◆) 0.3 mM, (○) 1 mM, and (■) 5 mM. The concentration of the PriA helicase is 1×10^{-6} M. The solid lines are nonlinear least-squares fits of the titration curves, according to the model of two different, discrete, and cooperative binding sites, defined by eqs 4−6 with the spectroscopic and binding parameters included in Table 3.

mental accuracy, the plots are linear in the examined salt concentration range. Furthermore, both binding constants decrease with increasing salt concentration. However, the slope $\partial \log K_{B_1}/\partial \log [NaCl] = -1.1 \pm 0.3$, while the slope $\partial \log K_{B_2}/\partial \log [NaCl] = -0.3 \pm 0.1$. These data indicate that, in examined solution conditions, a net release of ~1 ion accompanies nucleotide binding to the strong site, while the association of the cofactor with the weak binding site is accompanied by a much lower net ion release from the complex. The increase of salt concentration in solution does not affect to any detectable extent the cooperative interactions (data not shown). Within experimental accuracy, the value of $\sigma = 1.0 \pm 0.3$ in all of the examined [NaCl] (see the Discussion).

Effect of Magnesium on the Binding of Nucleotide Cofactors to the Two Nucleotide-Binding Sites on the PriA Helicase. Fluorescence titrations of PriA protein with TNP-ATP at two different protein concentrations in buffer C (pH 7.0, 20 °C) containing 20 mM NaCl and 0.1 mM EDTA are shown in Figure 7a. The maximum fluorescence quenching observed at saturation, $\Delta F_{max} = 0.77 \pm 0.05$. Notice, the high-affinity phase is not directly obvious in the titration curves. However, its presence is clearly detectable in the dependence of the observed relative fluorescence quenching, ΔF_{obs}, upon the total average degree of binding, $\Sigma\Theta_i$, of the TNP-ATP on the PriA helicase, shown in Figure 7b. The selected protein concentrations provide separation of the binding isotherms up to a fluorescence quenching value of ~0.28. The separation of the binding isotherms allows us to obtain the values of $\Sigma\Theta_i$ up to ~1.2 TNP-ATP molecules per PriA monomer. Extrapolation of the initial slope of the plot to $\Sigma\Theta_i = 1$ provides the quenching parameter, $\Delta F_1 = 0.18 \pm 0.03$. Thus, binding of the TNP-ATP molecule to the strong binding site induces only ~18% of the maximum quenching of the protein emission. The solid lines in Figure 7a are nonlinear least-squares fits of the spectroscopic titration curves using eqs 4−7 with a single set of parameters, $K_{B_1} = (1.0 \pm 0.3) \times 10^8$ M^{-1}, $K_{B_2} = (7.8 \pm 1.6) \times 10^5$ M^{-1}, $\sigma = 1.0 \pm 0.3$, $\Delta F_1 = 0.18 \pm 0.03$, and $\Delta F_2 = 0.59 \pm 0.05$ (Table 1). The solid line in Figure 7b is the theoretical dependence of the observed fluorescence quenching upon $\Sigma\Theta_i$, obtained using the same binding and spectroscopic parameters as in Figure 7a. Analogous titration curves for TNP-ADP binding PriA helicase are shown in Figure 8a. The solid lines in Figure 8a are nonlinear least-squares fits of the spectroscopic titration curves using eqs 4−7 with a single set of parameters, $K_{B_1} = (5.1 \pm 1.2) \times 10^7$ M^{-1}, $K_{B_2} = (3.7 \pm 1.1) \times 10^5$ M^{-1}, $\sigma = 1.0 \pm 0.3$, $\Delta F_1 = 0.20 \pm 0.03$, and $\Delta F_2 = 0.64 \pm 0.05$ (Table 1). Thus, in the absence of magnesium, the intrinsic affinities of the ADP analogue

Table 3: Thermodynamic Parameters, Intrinsic Binding Constants (K_1 and K_2), Cooperativity Parameter (σ), and Fluorescence Quenching Parameters (ΔF_1 and ΔF_2) for the Binding of TNP-ADP to Two Nucleotide Binding Sites of the *E. coli* PriA Helicase in Buffer C (pH 7.0, 20 °C), Containing 20 mM NaCl and Different $MgCl_2$ Concentrations

$MgCl_2$ (mM)	n	K_{B_1} (M^{-1})	K_{B_2} (M^{-1})	σ	ΔF_1	ΔF_2
0	2	$(5.1 \pm 1.2) \times 10^7$	$(3.7 \pm 1.1) \times 10^5$	1 ± 0.3	0.20 ± 0.03	0.64 ± 0.05
0.05	2	$(2.2 \pm 0.7) \times 10^6$	$(1.2 \pm 0.4) \times 10^5$	1 ± 0.3	0.40 ± 0.03	0.45 ± 0.04
0.1	2	$(2.5 \pm 0.9) \times 10^6$	$(1.3 \pm 0.4) \times 10^5$	1 ± 0.3	0.33 ± 0.03	0.52 ± 0.06
0.3	2	$(2.6 \pm 0.9) \times 10^6$	$(9.9 \pm 3.5) \times 10^4$	1 ± 0.3	0.30 ± 0.03	0.55 ± 0.07
1	2	$(2.0 \pm 0.7) \times 10^6$	$(5.0 \pm 1.5) \times 10^4$	1 ± 0.3	0.27 ± 0.03	0.58 ± 0.07
5	2	$(1.5 \pm 0.5) \times 10^6$	$(1.9 \pm 0.6) \times 10^4$	1 ± 0.3	0.20 ± 0.03	0.54 ± 0.08

strongly increase for both binding sites, by approximately a factor of 34 and 19, respectively, as compared to the intrinsic affinity in the presence of 5 mM $MgCl_2$ (Figure 1a). However, the cooperative interactions are not affected by the absence of magnesium.

Fluorescence titrations of the PriA helicase with TNP-ADP in buffer C (pH 7.0, 20 °C) containing 20 mM NaCl and different concentrations of $MgCl_2$ are shown in Figure 8b. The titration obtained in the absence of magnesium is also included. As the magnesium concentration increases, the curves are shifted toward higher TNP-ADP concentrations, indicating a decrease in the macroscopic affinity of the cofactor. The solid lines in Figure 8b are nonlinear least-squares fits of the spectroscopic titration curves using eqs 4−7. The obtained binding and spectroscopic parameters are included in Table 3. The two binding sites differ in their response to the presence of magnesium in solution. Interestingly, the most dramatic drop of the cofactor affinity, by a factor of ∼23, occurs at the strong nucleotide-binding site already at the lowest concentration of $MgCl_2 = 5 \times 10^{-5}$ M (see the Discussion). Also, the structure of the complex must be different at low [$MgCl_2$], as indicated by a higher value of ΔF_1, as compared to the value of the same parameter determined in the absence of magnesium and in the presence of a saturating concentration of magnesium (Table 3). Further increase in the magnesium concentration has little effect on the intrinsic affinity of the strong binding site. On the other hand, no dramatic change of the intrinsic affinity at low [$MgCl_2$] occurs at the weak site, where the value of the intrinsic binding constant, K_{B_2}, decreases by a factor of ∼3 at the lowest [$MgCl_2$] $= 5 \times 10^{-5}$ M and then gradually decreases with increasing magnesium concentration. However, similar to the strong binding site, magnesium affects the structure of the PriA−cofactor complex in the weak nucleotide-binding site, as indicated by the different ΔF_2 values (Table 3).

DISCUSSION

The PriA Helicase Has Two Nucleotide-Binding Sites. In this work, we describe extensive quantitative studies of the stoichiometry of the complex and the character of the binding process, including the intrinsic free energy of binding and cooperative interactions, in the nucleotide cofactor binding to the *E. coli* PriA helicase (*1*−*4*, *28*, *35*). The thermodynamic studies of the nucleotide binding to the PriA helicase have been greatly facilitated by the finding that the association of the nucleotide analogues, TNP-ADP and TNP-ATP, with the enzyme is accompanied by a strong quenching of the fluorescence of the enzyme (*17*). The TNP analogues of nucleotide cofactors prove to be very useful in examining the nucleotide cofactor interactions with different helicases (*28*, *31*, *40*, *47*−*49*). For instance, a similar strong quenching of the protein emission has been previously found in the case of the *E. coli* DnaB and the plasmid RSF1010 RepA protein hexameric helicases and was used by us to quantitatively examine the structure, thermodynamics, and kinetics of the DnaB helicase and RepA protein interactions with the nucleotide cofactors (*28*, *31*, *40*, *48*, *49*). The analogues bind strongly to the enzymes and allow the experimenter to detect the presence of the binding sites with intrinsic affinities characterized by binding constants of $\sim 10^2$ M^{-1} (*28*, *35*). Competition studies are then used to examine the binding of unmodified nucleotides with the enzyme (*28*, *35*, *42*−*44*, *48*, *49*).

Independent of any interaction models, binding of the TNP-ADP to the PriA helicase in applied solution conditions is clearly a biphasic process with strong and weak affinity binding phases (Figure 1a). As pointed out above, even more a pronounced biphasic character of the binding process is observed in the nucleotide association with the PriA−ssDNA complex (*64*). Examination of the high-affinity phase, using the quantitative fluorescence titration approach, reveals that in this phase a single TNP-ADP molecule binds to the enzyme (Figure 1b). However, this binding phase is characterized by an intermediate plateau at only 0.20 ± 0.03 of the quenching of the protein fluorescence. Independent analysis using the sedimentation velocity technique shows that ∼80% of the maximum saturation of the total binding process, 1.7 ± 0.2 TNP-ADP molecules, are associated with the PriA helicase (Figure 2). Thus, we have established that at saturation the PriA helicase binds two molecules of nucleotide cofactors.

The Primary Structure of the PriA Helicase Contains Three Putative Nucleotide-Binding Motifs. On the basis of the primary structure, the PriA protein contains seven "helicase motifs", and the enzyme is classified as a member of the SF2 super-family of helicases (*50*). Original analyses of the primary sequence of the gene product for the PriA helicase identified three sets of sequences that are putative nucleotide-binding motifs (*13*, *14*, *51*−*55*). The first motif is located at amino acid 224−231 at the N-terminus of the protein and contains a signature sequence, GX_4GKT, of the Walker motif A or phosphate binding loop (P-loop) in the N-terminus of the protein (*13*, *14*). The second sequence, of only partial match to the Walker motif B, RX_3GX_3-(hydrophobic amino acid)$_4$-D, through the sequence of -(hydrophobic amino acid)$_4$-D, includes amino acids 316−320 in the central region of the primary structure (*14*). However, the PriA helicase also contains a third sequence with a partial match to the Walker A motif as GX_5GKQ that includes amino acids 583−591 in the C-terminus of the

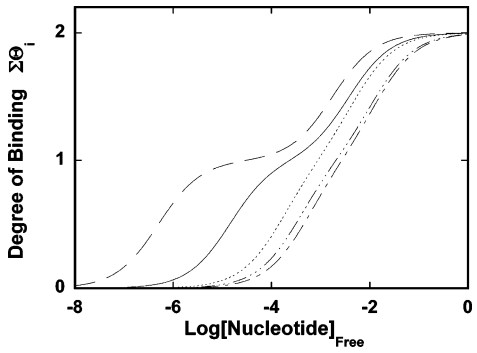

FIGURE 9: Theoretical dependence of the average degree of binding, $\Sigma\Theta_i$, for different nucleotide cofactors on the PriA helicase as a function of the logarithm of the free concentration of a nucleotide cofactor, using binding parameters obtained in this work (Table 2): (− − −) ADP, (—) ATP, (---) GDP, (− ---−) CDP, (− - −) TDP.

protein and is considered as a part of the helicase motif VI (*13*, *50*).

It should be stressed that the presence or absence of these motifs does not automatically imply the presence or absence of an actual nucleotide-binding site. Several proteins, known to bind nucleotide cofactors, do not possess even the canonical P-loop sequence (*52*−*54*). Nevertheless, such analysis is warranted, particularly, *in the context of the direct binding studies*, as discussed here. Thus, the discovery of two nucleotide-binding sites on the PriA helicase that can engage in interactions with the cofactor is consistent with the primary structure of the protein. The Walker A and B motifs have been found in several proteins to be two structural parts of a single nucleotide-binding site (*54*−*56*). Thus, the motif responsible for phosphate binding (Walker A) is placed in close spatial vicinity of the Walker B motif, which forms a hydrophobic pocket that can accommodate the base, preferably, adenine (*54*−*56*). It is then very probable that these two motifs form the strong nucleotide-binding site of the PriA helicase, highly specific for the adenosine nucleotides, as experimentally observed (Figure 1a, Table 2) (see below). The third motif, in the C-terminus of the protein, is a clear candidate for the location of the second, weak nucleotide-binding site (*13*). It is separated from the first two motifs by more than 250 amino acids and can easily form a discrete binding entity. Moreover, its sequence differs from the canonical Walker A motif, indicating that its properties and intrinsic affinity for the nucleotide cofactor should be different from the canonical Walker A motif, as also experimentally observed (Table 2) (*63*).

The Strong Nucleotide-Binding Site of the PriA Helicase Exhibits Dominant Preference for Adenosine Nucleotides, While the Weak Nucleotide-Binding Site Shows a Much Less Pronounced Base Specificity. The simplest statistical thermodynamic model that can describe the binding of the nucleotide cofactors to the PriA helicase is described by eqs 4−6. The model includes two discrete binding sites characterized by different intrinsic binding constants, K_{B_1} and K_{B_2} (see above). Any possible cooperative interactions between sites are characterized by the cooperative interaction parameter, σ. The dependence of the total average degree of binding, $\Sigma\Theta_i$, upon the logarithm of the free concentration of different nucleotide cofactors, shown in Figure 9, provides a direct comparison of the macroscopic affinities of the two nucleotide-binding sites of the PriA helicase. The plots have been obtained using the binding parameters from Table 2. Despite the presence of cooperative interactions, the difference in the behavior of the two nucleotide-binding sites is dramatic. The macroscopic affinity of ADP for the strong binding site is ∼2 and ∼3 orders of magnitude higher than the corresponding affinities for GDP and pyrimidine nucleotides, respectively. On the other hand, the weak nucleotide-binding site shows only a factor of ∼3 preference for ADP over GDP and less than an order of magnitude higher macroscopic affinity over other cofactors (Figure 9).

Such behavior would be expected if, as discussed above, the strong site is built of the Walker A and B motifs that provide both affinity and specificity for adenine nucleotides, while a much less specific version of the P-loop in the weak binding site responds predominantly to the phosphate groups and ribose region of the cofactor (see below). In a companion paper (*63*), we show that the nucleotide cofactor binding to the weak binding site of the PriA helicase is described by a simpler kinetic mechanism as compared with the complex multistep mechanism observed for the strong site, thus supporting this conclusion. Moreover, a much lower increase of the fluorescence from the TNP moiety in the intermediates of the association process with the weak nucleotide-binding site, as compared to the strong site, indicates a much less hydrophobic character of the site. This behavior is very different from the *E. coli* primary replicative helicase, the DnaB protein, which shows a much less pronounced preference for the purine nucleotide cofactors, both ADP and GDP, over the pyrimidine cofactors (*28*, *44*). Notice, the primary structure of the DnaB helicase does not contain the Walker B motif and the affinity of its nucleotide-binding site, containing only a partial match to the Walker A motif, is little dependent on the type of the base of the cofactor (*28*, *44*). Current data indicate that the PriA helicase can hydrolyze NTPs independently of the type of base, although with very different specific activities (*9*, *19*). The equilibrium studies, reported here, point out an important caveat in such studies. Quantitative comparison between different NTPase activities should by performed at the saturation of one or both nucleotide-binding sites of the enzyme rather than at the same concentration of the cofactors. Otherwise, instead of different specific activities, the activities of the enzyme differently saturated with the cofactors will be observed.

The Intrinsic Affinities of the Two Nucleotide-Binding Sites of the PriA Helicase Are Affected Differently by the Structure of the Phosphate and Ribose Regions of the ATP Cofactor. The obtained data indicate that the intrinsic affinity of various ATP analogues for the strong nucleotide-binding site of the PriA helicase is much more dependent on the structure of the phosphate groups than the intrinsic affinity of the weak nucleotide-binding site (Table 2). Thus, ATP binds to the strong nucleotide-binding site with an intrinsic affinity that is a factor of ∼8 higher than ATPγS and a factor of ∼23 higher than AMP-PCP. However, in the case of the weak binding site, ATPγS has an intrinsic affinity even higher than ATP, while the intrinsic affinity of AMP-PNP and AMP-PCP are only a factor of ∼4 lower than ATP. Because the type of base is identical for all examined cofactors, these findings strongly suggest that the phosphate binding regions of the two binding sites are different. In other words, these

data corroborate well with the conclusion that different nucleotide-binding motifs are involved in the structures of the two binding sites of the enzyme (see above). The strong binding site with its canonical P-loop and adenine-specific hydrophobic pocket should be more restrictive in acceptance of triphosphate group differing from ATP (*54*, *55*). In the case of dATP, the structure of the phosphate group is the same as in ATP, but the dATP affinities are higher for both binding sites than that of ATP, indicating that the strong site responds to all three major regions (base, phosphate group, sugar) of the cofactor while the weak site senses mainly the phosphate group and sugar of the bound nucleotide.

The Presence of Cooperative Interactions Indicate Communication between the Two Nucleotide-Binding Sites of the PriA Helicase. Although the TNP-ADP and TNP-ATP analogues can detect the presence of the weak nucleotide-binding site, in the concentration range of the cofactor that is amenable for quantitative studies (Figure 1a), their binding process is characterized by a cooperative interaction parameter, $\sigma = 1.0 \pm 0.3$, indicating an apparent lack of significant cooperative interactions between the two nucleotide-binding sites (Table 1). However, clear shift of the competition titration curves toward lower reference ligand (TNP-ADP) concentration in the presence of unmodified nucleotides, independent of any binding model, indicates the presence of positive cooperative interactions between the cofactor molecules bound to the helicase (Figure 4) (*42*, *43*). In the examined solution conditions, the value of σ for different nucleotides is in the range of ∼3.3−5.0. Thus, although the values of the cooperativity parameter, σ, are moderate, they clearly indicate the presence of communication between the two nucleotide-binding sites of the PriA helicase.

The Cooperative Interactions Are Not Dependent on the Type of Base and Structure of the Phosphate Region of the Nucleotide Cofactor. Unlike the intrinsic affinities, the type of the base of the nucleotide cofactor and the structure of the phosphate group of the ATP analogues do not significantly affect the cooperative interactions between the two nucleotide-binding sites of the PriA helicase (Table 2). With the exception of ATPγS, the value of σ_C changes from 3.0 ± 1.5 for AMP-PNP to 5.0 ± 2.6 for GDP. Such results indicate that the cooperative interactions are predominantly generated through the phosphate binding motifs of the nucleotide-binding sites. However, the fact that TNP analogues, where the TNP group is located on the ribose, are both characterized by $\sigma = 1.0 \pm 0.3$ strongly suggest that the ribose region of the cofactor is also involved. Similar behavior has been previously observed for the DnaB helicase where the negative cooperative interactions between the nucleotide-binding sites of the hexamer were independent of the type of base but dependent upon the structure of the phosphate and ribose region of the bound nucleotide (*28*,*44*).

Salt Effect on the Nucleotide Cofactor Binding to the PriA Helicase Indicates a Different Nature of the Two Nucleotide-Binding Sites on the Enzyme. Additional information about the nature of the two nucleotide-binding sites of the PriA helicase comes from the examined salt effect on the cofactor binding (Figure 6). The slope $\partial \log K_1/\partial \log [NaCl] = -1.1 \pm 0.3$, indicating a net release of ∼one ion accompanying the cofactor binding to the strong nucleotide-binding sites (*45*, *46*). The linear character of the plot would suggest a simple competition between the phosphate and Cl^- anions for a positively charged site in the binding site. On the other hand, increasing the salt concentration causes an initial increase of the relative fluorescence quenching followed by a decrease of the quenching, accompanying the cofactor binding to the strong binding site (Figure 6a). Because the relative quenching of ∼0.2−0.3, accompanying the binding to the strong site, reflects the state of at least 3−5 tryptophan residues out of 15 tryptophan residues of the helicase, the observed nonlinear salt effect suggests that binding of ions to the protein at some distance from the nucleotide-binding site participates in the ion exchange process (Figure 6a). Much lower values of the slope, $\partial \log K_2/\partial \log [NaCl] = -0.3 \pm 0.1$, clearly indicates a very different character of interactions between the cofactor and the protein matrix in the weak nucleotide-binding site. Moreover, the nonlinear effect on the observed relative fluorescence quenching accompanying the binding to the weak binding site, analogous to the effect observed for the strong binding site, also indicates that ion binding to the protein is a part of the thermodynamic response of interactions at the weak site to the changes in [NaCl] concentration. The lack of any detectable salt effect on cooperative interactions as compared to the two intrinsic binding processes is surprising and suggests compensatory effects comprising both ion release and uptake (*45*, *46*).

The Intrinsic Affinities of ATP for the Strong and Weak Binding Sites of the PriA Helicase Are Lower Than the Intrinsic Affinities of ADP. As mentioned above, because PriA helicase does not hydrolyze ATP to any detectable extent in the absence of the DNA, on the time scale of the binding experiments, we could determine both the intrinsic affinities for ATP, ADP, and inorganic phosphate for the enzyme. In the presence of magnesium, the intrinsic binding constant of ATP for the strong nucleotide binding site is by a factor of ∼29 lower than the value observed for ADP, although it is higher by approximately 3 orders of magnitude than the affinity of the PO^{4-} group (Table 2). Lower affinities of ATP and its hydrolysis product, ADP, is not expected for an enzyme that performs free energy transduction because the strong ATP binding as compared to both hydrolysis products would allow the enzyme to hydrolyze ATP in the active site with a very low change in the free energy and store the free energy of ATP hydrolysis (*57*, *58*). In the case of the *E.* coli DnaB and plasmid RSF1010 RepA helicases, the obtained data indicate that the ATP affinity is also lower than the affinity of ADP (*38*, *44*, *48*, *49*, *61*, *62*). However, the ATP hydrolysis in the active site of the DnaB helicase is still characterized by a very low equilibrium constant (∼2), indicating that the reaction in the active site releases much less free energy than the same reaction in solution (*58*). The data on ATP, ADP, and PO^{4-} group binding, now available for the PriA, DnaB, and RepA helicases, strongly suggest that the mechanism of storing the energy of ATP hydrolysis by helicases, which can be used to perform the dsDNA unwinding and mechanical work of translocation along the DNA lattice, may be in some aspects different from the mechanism proposed, for example, myosin (*57*, *58*). By the same token, the ATPase activities of helicases are additionally activated in the complex with the ssDNA, albeit the energetics and kinetics of ATP, ADP, and PO^{4-} group binding to a helicase, bound to the DNA are not currently known for any helicase. As we proposed before, it is possible

that a helicase acquires free-energy transducing capabilities, similar to myosin, when associated with the ssDNA, thus forming a "holoenzyme" (*21*, *22*, *44*). The results on ATP, ADP, and PO^{4-} group binding, now available for three different helicases, strongly suggest such a possibility.

Binding of Magnesium Cations to the PriA Helicase Affects Predominantly the Intrinsic Affinity of the Nucleotide Cofactor Binding to the Strong Nucleotide-Binding Site of the Helicase. The magnesium effect on cofactor binding to the PriA protein is different from the salt effect, discussed above. In the case of the strong nucleotide-binding site, there is a large decrease in the intrinsic nucleotide affinity, from $K_{B_1} = 5.1 \times 10^7\ M^{-1}$ in the absence of $MgCl_2$ to $K_{B_1} = 2.2 \times 10^6\ M^{-1}$ at the lowest $MgCl_2$ concentration examined (5×10^{-5} M), followed by only a slight, if any, further decrease of K_{B_1} at saturating [$MgCl_2$] (Table 3). In other words, the magnesium effect on the strong nucleotide binding site includes magnesium binding site(s) that must have an affinity higher than $\sim 10^5 - 10^6\ M^{-1}$. Similar increases in affinity in the absence of magnesium are observed for the ATP analogue (Table 1), although we could not examine the binding of this cofactor at different [$MgCl_2$] due to efficient hydrolysis of TNP-ATP in the presence of Mg^{2+} (see above, *63*). Because, in the applied solution conditions, the magnesium affinity for the nucleotide cofactor is in the range of $\sim 10^4 - 10^5\ M^{-1}$, the simplest explanation of the observed effect is that the large decrease in the value of K_{B_1} at low [$MgCl_2$] results from the difference between the affinity of the free cofactor and its magnesium form (*48*, *49*, *60*). In other words, magnesium-free TNP-ADP associates with the strong binding site on PriA with an intrinsic binding constant that is a factor of ~23 higher than the binding constant for the Mg^{2+}-TNP-ADP complex. In the case of the weak binding site, the difference between the intrinsic affinities for the free cofactor versus its magnesium complex is much less pronounced with the affinity decreasing only by a factor of ~3 when Mg^{2+} is removed (Table 3). Also, contrary to the strong binding site, further increase of magnesium concentration leads to further decrease of the intrinsic affinity for the weak site. These results are unexpected; rather an opposite effect, an increased intrinsic affinity for both nucleotide-binding sites in the presence of Mg^{2+}, would be anticipated as the magnesium cations are necessary for the ATPase activity of the enzyme. The pronounced effect of magnesium on the intrinsic affinity of the nucleotide cofactor for the strong nucleotide-binding site indicates that Mg^{2+} cations are specifically involved in controlling the cofactor affinity for the strong site, while the association with the weak site is predominantly determined by interactions between the phosphate groups and ribose region of the cofactor with the protein matrix (see above). In the context of the fact that magnesium is necessary for catalysis and the strong nucleotide-binding site has overwhelming preference for the adenine nucleotides, the specific effect of magnesium on the strong site also suggests that the site is the dominant ATPase site of the enzyme (see below).

Functional Implications. Thermodynamic studies described in this work shed light on several properties of the PriA helicase observed in previous biochemical studies (*19*, *20*). Moreover, comparison of the thermodynamic data with biochemical activities of the PriA provides additional clues on the character and role of the two nucleotide-binding sites of the enzyme. Mutations of the conserved lysine in the canonical Walker A motif, GX_4GKT, located at the N-terminus of the protein completely abolished the examined NTPase activity of the protein (*19*). Furthermore, the experiments were performed at an ATP concentration where thermodynamic results, discussed here, indicate that only the strong nucleotide-binding site engages in interactions with ATP (Table 2, Figure 9). Although at present it is not clear whether the catalysis and/or the affinity of ATP is affected by the mutations, both thermodynamic and biochemical data convincingly indicate that the strong nucleotide-binding site is located at the N-terminus of the protein (i.e., Walker A and B motifs are indeed forming the ATP-specific, strong nucleotide-binding site). Second, despite the mutations, the variants preserve their activities in ATP-dependent assembly of the primosome, suggesting that the weak nucleotide-binding site of the PriA protein is sufficient for the assembly activity of the enzyme. Interestingly, the examined variants of the enzyme, with abolished ATP hydrolysis/binding capability at the strong nucleotide-binding site, seem to bind even stronger to the nucleic acid (*19*).

Thermodynamic data also provide an explanation for another puzzling result with regard to the PriA helicase (*20*). It has been observed that at low ATP concentrations ($\sim 10^{-4}$ M), the enzyme can efficiently unwind only short dsDNA fragments. On the other hand, the helicase is capable of unwinding long stretches (~400 bps) of the dsDNA at ~10-fold higher ATP concentrations. Although the solution conditions were different from the conditions applied in our work, these data strongly suggest that at low [ATP], where predominantly the strong nucleotide-binding site is saturated with the cofactor, the PriA helicase has a lower unwinding activity and/or a lower unwinding processivity (*61*,*62*). At increased [ATP], binding of the cofactor to the weak nucleotide-binding site increases the efficiency of unwinding. In other words, the weak nucleotide-binding site seems to play a role of a processivity-control element of the enzyme, while the strong binding site is the major ATPase site that provides energy for translocation and dsDNA unwinding. Quantitative studies of the PriA helicase binding to the ssDNA encompassing the proper and the total DNA-binding site of the enzyme strongly support that conclusion (*64*).

ACKNOWLEDGMENT

We thank Betty Sordahl for reading the manuscript.

REFERENCES

1. Marians, K. J. (1992) Prokaryotic DNA replication, *Annu. Rev. Biochem. 61*, 673−719.
2. Marians, K. J. (1999) PriA: at the crossroads of DNA replication and recombination, *Prog. Nucleic Acid Res. Mol. Biol. 63*, 39−67.
3. Kornberg, A., and Baker, T. A. (1992) *DNA Replication*, pp 275−293, Freeman, San Francisco.
4. Sangler, S. J., and Marians, K. J. (2000) Role of PriA in replication fork reactivation in *Escherichia coli*, *J. Bacteriol. 182*, 9−13.
5. McMacken, R., Ueda, K., and Kornberg, A. (1977) Migration of *Escherichia coli* dnaB protein on the template DNA strand as a mechanism in initiating DNA replication, *Proc. Natl. Acad. Sci. U.S.A. 74*, 4190−4194.
6. Wickner, S., and Hurwitz, J. (1975) Association of phiX174 DNA-dependent ATPase activity with an *Escherichia coli* protein, replication factor Y, required for in vitro synthesis of phiX174 DNA, *Proc. Natl. Acad. Sci. U.S.A. 72*, 3342−3346.

7. Shlomai, J., and Kornberg, A. (1980) A prepriming DNA replication enzyme of *Escherichia coli*. I. Purification of protein n′: a sequence-specific, DNA-dependent ATPase, *J. Biol. Chem. 255*, 6789−6793.
8. Zipursky, S. L., and Marians, K. J. (1980) Identification of two *Escherichia coli* factor Y effector sites near the origins of replication of the plasmids ColE1 and pBR322, *Proc. Natl. Acad. Sci. U.S.A. 77*, 6521−6525.
9. Shlomai, J., and Kornberg, A. (1980) A prepriming DNA replication enzyme of *Escherichia coli*. II. Actions of protein n′: a sequence-specific, DNA-dependent ATPase, *J. Biol. Chem. 255*, 6794−6798.
10. Marians, K. J., Soeller, W., and Zipursky, S. L. (1982) Maximal limits of the *Escherichia coli* replication factor Y effector site sequences in pBR322 DNA, *J. Biol. Chem. 257*, 5656−5662.
11. Lee, M. S., and Marians, K. J. (1987) *Escherichia coli* replication factor Y, a component of the primosome, can act as a DNA helicase, *Proc. Natl. Acad. Sci. U.S.A. 84*, 8345−8349.
12. Lasken, R. S., and Kornberg, A. (1988) The primosomal protein n′ of *Escherichia coli* is a DNA helicase, *J. Biol. Chem. 263*, 5512−5518.
13. Nurse, P., DiGate, R. J., Zavitz, K. H., and Marians, K. J. (1990) Molecular cloning and DNA sequence analysis of *Escherichia coli* priA, the gene encoding the primosomal protein replication factor Y, *Proc. Natl. Acad. Sci. U.S.A. 87*, 4615−4619.
14. Lee, E. H., Masai, H., Allen, G. C., Jr., and Kornberg, A. (1990) The priA gene encoding the primosomal replicative n′ protein of *Escherichia coli*, *Proc. Natl. Acad. Sci. U.S.A. 87*, 4620−4624.
15. McGlynn, P., Al-Deib, A. A., Liu, J., Marians, K. J., and Lloyd, R. G. (1997) The DNA replication protein PriA and the recombination protein RecG bind D-loops, *J. Mol. Biol. 270*, 212−221.
16. Nurse, P., Liu, J., and Marians, K. J. (1999) Two modes of PriA binding to DNA, *J. Biol. Chem. 274*, 25026−25032.
17. Jones, J. M., and Nakai, H. (1999) Duplex opening by primosome protein PriA for replisome assembly on a recombination intermediate, *J. Mol. Biol. 289*, 503−516.
18. Jones, J. M., and Nakai, H. (2001) *Escherichia coli* PriA helicase: fork binding orients the helicase to unwind the lagging strand side of arrested replication forks, *J. Mol. Biol. 312*, 935−947.
19. Zavitz, K. H., and Marians, K. J. (1992) ATPase-deficient mutants of the *Escherichia coli* DNA replication protein PriA are capable of catalyzing the assembly of active primosome, *J. Biol. Chem. 267*, 6933−6940.
20. Lee, M. S., and Marians, K. J. (1990) Differential ATP requirements distinguish the DNA translocation and DNA unwinding activities of the *Escherichia coli* PriA protein, *J. Biol. Chem. 265*, 17078−17083.
21. Jezewska, M. J., Rajendran, S., and Bujalowski, W. (2000) *Escherichia coli* replicative helicase PriA protein-single-stranded DNA complex. Stoichiometries, free energy of binding, and cooperativities, *J. Biol. Chem. 275*, 27865−27873.
22. Jezewska, M. J., and Bujalowski, W. (2000) Interactions of *Escherichia coli* replicative helicase PriA protein with single-stranded DNA, *Biochemistry 39*, 10454−10467.
23. Lohman, T. M., and Bjornson, K. P. (1996) Mechanisms of helicase-catalyzed DNA unwinding, *Annu. Rev. Biochem. 65*, 169−214.
24. von Hippel, P. H. and Delagoutte, E. (2002) Helicase mechanisms and the coupling of helicases within macromolecular machines. Part I: structures and properties of isolated helicases, *Q. Rev. Biophys. 35*, 431−78.
25. von Hippel, P. H., and Delagoutte, E. (2003) Helicase mechanisms and the coupling of helicases within macromolecular machines. Part II: integration of helicases into cellular processes, *Q. Rev. Biophys. 36*, 1−69.
26. Edeldoch, H. (1967) Spectroscopic determination of tryptophan and tyrosine in proteins, *Biochemistry 6*, 1948−1954.
27. Gill, S. C., and von Hippel, P. H. (1989) Calculation of protein extinction coefficients from amino acid sequence data, *Anal. Biochem. 182*, 319−326.
28. Bujalowski, W. and Klonowska, M. M. (1993). Negative cooperativity in the binding of nucleotides to *Escherichia coli* replicative helicase DnaB protein. Interactions with fluorescent nucleotide analogs, *Biochemistry 32*, 5888−5900.
29. Galletto, R., Rajendran, S., and Bujalowski, W. (2000). Interactions of nucleotide cofactors with the *Escherichia coli* replication factor DnaC protein, *Biochemistry 39*, 12959−12969.
30. Hiratsuka, T. (1983) New ribose-modified fluorescent analogs of adenine and guanine nucleotides available as substrates for various enzymes, *Biochim. Biophys. Acta 742*, 496−508.
31. Bujalowski, W., and Klonowska, M. M. (1994) Structural characteristics of the nucleotide-binding site of *Escherichia coli* primary replicative helicase DnaB protein. Studies with ribose and base-modified fluorescent nucleotide analogs, *Biochemistry 33*, 4682−4694.
32. Bujalowski, W., and Jezewska, M. J. (1995) Interactions of *Escherichia coli* primary replicative helicase DnaB protein with single-stranded DNA. The nucleic acid does not wrap around the protein hexamer, *Biochemistry 34*, 8513−8519.
33. Jezewska, M. J., and Bujalowski, W. (1997) Quantitative analysis of ligand−macromolecule interactions using differential quenching of the ligand fluorescence to monitor the binding, *Biophys. Chem. 64*, 253−269.
34. Lakowicz, J. R. (1999) *Principles of Fluorescence Spectroscopy*, pp 25−61, Plenum Press, New York.
35. Bujalowski, W., and Jezewska, M. J. (2000) in *Spectrophotometry & Spectrofluorimetry. A Practical Approach* (Gore, M. G. Ed.), pp 141−165, Oxford University Press, Oxford.
36. Lohman, T. M., and Bujalowski, W. (1991) Thermodynamic methods for model-independent determination of equilibrium binding isotherms for protein−DNA interactions: spectroscopic approaches to monitor binding, *Methods Enzymol. 208*, 258−290.
37. Bujalowski, W., Klonowska, M. M., and Jezewska, M. J. (1994) Oligomeric structure of *Escherichia coli* primary replicative helicase DnaB protein, *J. Biol. Chem. 269*, 31350−31358.
38. Jezewska, M. J., and Bujalowski, W (1996) Global conformational transitions in *E. coli* primary replicative DnaB protein induced by ATP, ADP and single-stranded DNA binding, *J. Biol. Chem. 271*, 4261−4265.
39. Galletto, R., Jezewska, M. J., and Bujalowski, W. (2003) Interactions of the *Escherichia coli* DnaB helicase hexamer with the replication factor the DnaC protein. Effect of nucleotide cofactors and the ssDNA on protein−protein interactions and the topology of the complex, *J. Mol. Biol. 329*, 441−465.
40. Bujalowski, W., and Klonowska, M. M. (1994) Close proximity of tryptophan residues and ATP-binding site in *Escherichia coli* primary replicative helicase DnaB protein. Molecular topography of the enzyme, *J. Biol. Chem. 269*, 31359−31371.
41. Hill, T. L. (1985). *Cooperativity Theory in Biochemistry. Steady State and Equilibrium Systems*, pp 167−234, Springer-Verlag, New York.
42. Jezewska, M. J., and Bujalowski, W, (1998) A general method of analysis of ligand binding to competing macromolecules using the spectroscopic signal originating from a reference macromolecule. application to *Escherichia coli* replicative helicase DnaB protein−nucleic acid interactions, *Biochemistry 35*, 2117−2128.
43. Jezewska, M. J., Galletto, R., and Bujalowski, W. (2003) Rat Pol β binds double-stranded DNA using exclusively the 8-kDa domain. Stoichiometries, intrinsic affinities, and cooperativities, *Biochemistry 42*, 5955−5970.
44. Jezewska, M. J., Kim, U.-S., and Bujalowski, W. (1996) Interactions of *Escherichia coli* primary replicative helicase DnaB protein with nucleotide cofactors, *Biophys. J. 71*, 2075−2086.
45. Record, M. T., Jr., Anderson, C. F., and Lohman, T. M. (1978) Thermodynamic analysis of ion effects on the binding and conformational equilibria of proteins and nucleic acids: the roles of ion association or release, screening, and ion effects on water activity, *Q. Rev. Biophys. 11*, 103−178.
46. Record, M. T., Lohman, T. M., and deHaseth, P. L. (1976) Ion effects on ligand−nucleic acid interactions, *J. Mol. Biol. 107*, 145−158.
47. Huang, S. G., K. Weisshart, and E. Fanning (1998) Characterization of the nucleotide binding properties of SV40 T antigen using fluorescent 3′(2′)-*O*-(2,4,6-trinitrophenyl)adenine nucleotide analogues, *Biochemistry 37*, 15336−44.
48. Jezewska, M. J., Lucius, A. L., and Bujalowski, W. (2005) Binding of six nucleotide cofactors to the hexameric helicase RepA protein of plasmid RSF1010. 1. Direct evidence of cooperative interactions between the nucleotide-binding sites of a hexameric Helicase, *Biochemistry 44*, 3865−3876.
49. Jezewska, M. J., Lucius, A. L., and Bujalowski, W. (2005) Binding of six nucleotide cofactors to the hexameric helicase RepA protein of plasmid RSF1010. 2. Base specificity, nucleotide structure, magnesium, and salt effect on the cooperative binding of the cofactors, *Biochemistry 44*, 3877−3890.

50. Gorbalenya, A. E., and E. V. Koonin (1993) Helicases: amino acid sequence comparisons and structure−function relationships, *Curr. Opin. Struct. Biol. 3*, 419−429.
51. Walker, J. E., Saraste, M., Runswick, M. J., and Gay, N. J. (1983) Distantly related sequences in the α- and β-subunits of ATP synthase, myosin, kinases, and other ATP-requiring enzymes and a common nucleotide binding fold, *EMBO J. 1*, 945−951.
52. Saraste, M., Sibbald, P. R., and Wittinghofer, A. (1990) The P-loop−a common motif in ATP- and GTP-binding proteins, *Trends Biochem. Sci, 5*, 430−432.
53. Taylor, W. R., and Green, N. M. (1989) The predicted secondary structures of the nucleotide-binding sites of six cation-transporting ATPases lead to a probable tertiary fold, *Eur. J. Biochem. 179*, 241−8.
54. Doolittle, R. F., Johnson, M. S., Husain, I., Houten, B., Thomas, D. C., and Sancar, A. (1986) Domainal evolution of the a prokaryotic DNA repair protein and is relationship to active-transport proteins, *Nature 323*, 451−453.
55. Myles. G. M., Hearst, J. E., and Sancar, A. (1991) Site-specific mutagenesis of conserved residues within Walker A and B sequences of *Escherichia coli* UvrA protein, *Biochemistry 30*, 3824−3834.
56. Korolev, S., Hsieh J., Gauss, G. H., Lohman, T. M., and Waksman, G. (1997) Major domain swiveling revealed by the crystal structures of complexes of *E. coli* Rep helicase bound to single-stranded DNA and ADP, *Cell 90*, 635−47.
57. Jencks, W. P. (1980) The utilization of the binding energy in coupled vectorial processes, *Adv. Enzymol. 51*, 75−106.
58. Jencks, W. P. (1981) On the attribution and additivity of binding energies, *Proc. Natl. Acad. Sci. U.S.A. 78*, 4046−4050.
59. Rajendran, S., Jezewska, M. J.; Bujalowski W. (2000). Multiple-step kinetic mechanism of DNA-independent ATP binding and hydrolysis by *Escherichia coli* replicative helicase DnaB protein: quantitative analysis using the rapid quench-flow method, *J. Mol. Biol. 303*, 773−795.
60. Garfinkel, L., and Garfinkel, D. (1984) Calculation of free-Mg^{2+} concentration in adenosine 5′-triphosphate containing solutions in vitro and in vivo, *Biochemistry 23*, 3547−3552.
61. Galletto, R., Jezewska, M. J., and Bujalowski, W. (2004) Unzipping mechanism of the double-stranded DNA unwinding by a hexameric helicase. Quantitative analysis of the rate of the dsDNA unwinding, processivity and kinetic step-size of the *Escherichia coli* DnaB helicase using rapid quench-flow method, *J. Mol. Biol. 343*, 83−99.
62. Galletto, R., Jezewska, M. J., and Bujalowski, W. (2004) Unzipping mechanism of the double-stranded DNA unwinding by a hexameric helicase. The effect of the 3′ arm and the stability of the dsDNA on the unwinding activity of the *Escherichia coli* DnaB helicase, *J. Mol. Biol. 343*, 101−114.
63. Lucius, A. L., Jezewska, M. J., Roychowdhury, A., and Bujalowski, W. (2006) Kinetic mechanisms of the nucleotide cofactor binding to the strong and weak nucleotide-binding site of the *Escherichia coli* PriA helicase. 2, *Biochemistry 45*, 7217−7236.
64. Lucius, A. L., Jezewska, M. J., and Bujalowski, W. (2006) Allosteric interactions between the nucleotide-binding sites and the ssDNA-binding site in the PriA helicase−ssDNA complex. 3, *Biochemistry 45*, 7237−7255.

BI051826M